Microstructure and properties of Ni–Mn–Ga alloys produced by rapid solidification and pulsed electric current sintering

Outi Söderberg [a,*], David Brown [b], Ilkka Aaltio [a], Jussi Oksanen [a], Jesse Syrén [a], Heikki Pulkkinen [a], Simo-Pekka Hannula [a]

[a] Department of Materials Science and Engineering, Aalto University, School of Chemical Technology, P.O. Box 16200, FI-00076 Aalto, Finland
[b] Magnequench Technology Centre, 61 Science Park Road, #01-19 Galen, Singapore Science Park II, Singapore 117525, Singapore

ARTICLE INFO

ABSTRACT

Ni–Mn–Ga alloys were compacted using pulsed electric current sintering (PECS) at 850–875 °C (50 MPa, 8 min) of flake-like powders made from the rapidly quenched melt-spun ribbons. Two kinds of ribbons were used: one made with a relatively slow wheel speed (6 m/s; average grain size ~14 μm), and another with a faster wheel speed (23 m/s; average grain size ~5 μm). Both sets of flake-like powders consisted of a mixture of non-modulated martensite (NM) and seven-layered modulated martensite (7M) structure. The amount of NM was greater in the slower speed material, while the other one exhibited mostly the 7M structure. These crystal structures were inherited by the sintered samples. In the compacts having the NM structure the multi-step martensitic reaction overlapped with the magnetic transition, and the Curie temperatures during heating and cooling differed from each other. In the compacts having mainly 7M structure the Curie point was about 100 °C and the martensitic transition took place in the paramagnetic state, while the intermartensitic one occurred in the region of 60–85 °C. This material demonstrated good magnetic properties and saturation magnetization, at best ~50 emu/g. Mechanical properties of the compacts were good, and comparable to those of the polycrystalline Ni–Mn–Ga samples in compression.

1. Introduction

Ni–Mn–Ga alloys have been studied intensively because of their great potential for actuator and sensor applications, as well as high temperature shape memory, vibration damping and magnetocaloric devices [1]. In terms of the applications their crystal structure is of major importance. The five-layered 5M and seven-layered 7M modulated martensites (also referred to 10M and 14M martensites, respectively) having a twin structure that can be reoriented with the magnetic field or mechanical loading are suitable for the actuators [2–4], while the non-modulated martensitic structures are the best for the conventional shape memory use [5]. Furthermore, when the magnetic transition and the phase transformations overlap, material has potential for the magnetocaloric applications [6]. Conventional processing of these materials takes place via a melt route including casting of the polycrystalline master alloy with correct chemical composition and growing of the

single crystal. There is a strong segregation tendency in these alloys [7,8], and therefore long homogenizing and ordering heat treatments are required before their use [9,10]. This conventional fabrication process is costly and time consuming, and thus, other possible fabrication routes are of interest.

Melt-spinning technology is an efficient and fast preparation technique of polycrystalline ribbons. It is capable of producing materials with a high degree of structural uniformity and fine grain structure. Melt-spinning is used commercially to produce nanocrystalline Nd-Fe-B powders for permanent magnets [11,12]. Rapidly quenched Ni–Mn–Ga ribbons have been used for the thin film applications and composite structures and their structural and magnetic behavior has been studied quite intensively [13–20]. However, the size of the melt-spun ribbon as such does not meet the demands of the large-dimensional applications.

For the compaction of ribbons pulsed electric current sintering (PECS) – also called spark plasma sintering (SPS) or field assisted sintering technique (FAST) is an interesting option. Sintering is aided by high current pulses generating direct Joule heating in the die and sample material allowing high heating rates, relatively low overall processing temperature and short processing time, thus, minimizing the influence of the different diffusion mechanisms and grain growth [21]. Applied pressure enhances the contact between the particles and helps to obtain dense materials. However, in order

* Corresponding author. Tel.: +358 9 47022681; fax: +358 9 47022677.
 E-mail addresses: outi.soderberg@tkk.fi (O. Söderberg),
dbrown@magnequench.com (D. Brown), ilkka.aaltio@tkk.fi (I. Aaltio),
joksanen@cc.hut.fi (J. Oksanen), jesse.syren@carbodeon.fi (J. Syrén),
heikki.pulkkinen@tkk.fi (H. Pulkkinen), simo-pekka.hannula@tkk.fi (S.-P. Hannula).

Table 1
Properties of the powders, processing parameters, and properties of the compacted samples.

Powder				Applied sintering parameters temperature; dwell time; pressure	Compacted sample		
Cooling speed	Chemical composition (wt%)	Grain size (μm)			Density Archimedes (g/cm^3)	Theoretical density (TD) reference 8.1 (g/cm^3)	Grain size (μm)
6 m/s	54.58 Ni–21.51 Mn–23.27 Ga–0.03 O–0.01 C	14	NM 1	850 °C; 8 min; 50 MPa	7.996	98.7%	21
			NM 2	875 °C; 8 min; 50 MPa	8.054	99.4%	22
23 m/s	53.74 Ni–21.79 Mn–24.34 Ga–0.01 O	5	7M1		8.066	99.6%	9
			7M2		8.092	99.9%	9

to sustain the properties of the raw material, one should avoid melting the material, which may turn out to be a problem, since in the metallic materials local melting may take place clearly below the melting temperature of the bulk [22].

So far, there are only a few publications of using PECS for the Ni–Mn–Ga powders. Wang et al. [23] applied PECS process on crushed arc-melted polycrystalline austenitic alloy, using 900 °C for 8–10 min in vacuum. Sintered austenitic material was annealed at 800 °C for 10 days to reveal the distinct phase transformation behavior. The sintered material showed better mechanical behavior than the arc-melted one. Compression yield-stress, fracture strength, true fracture strength, and strain were 592 MPa, 1760 MPa, 1540 MPa and 14.2% correspondingly for the sintered one and 437 MPa, 605 MPa, 595 MPa, and 1.5% for the arc-melted one [24]. Also, Matsumoto et al. [25] crushed powders from the arc melted alloys $Ni_{2.1}Mn_{0.9}Ga$ and $Ni_{2.18}Mn_{0.82}Ga$, and PECS processed them at 1000 °C under 48.5 MPa. Sintered materials showed the same transition temperatures as the arc melted raw materials, i.e. the transformation temperatures of the alloy $Ni_{2.1}Mn_{0.9}Ga$ were close to 0 °C (austenite at RT) the Curie point being 77 °C, while the alloy $Ni_{2.18}Mn_{0.82}Ga$ was martensitic at room temperature, since its structural and magnetic transition temperatures were around 65 °C [26]. In these works somewhat different values for the Young's modulus (E) at room temperature were obtained. The as-sintered austenitic material had E of 106.6 GPa and the Poisson ratio of 0.38 in [24], while the modulus was 40 GPa for the sintered and 10 GPa for arc melted alloys in [27]. Softening close to the phase transformation temperature has been reported in Ref. [27]. E decreases when the reverse transformation is approached, while at −100 °C the E of the martensitic $Ni_{2.18}Mn_{0.82}Ga$ structure was larger than that of the $Ni_{2.1}Mn_{0.9}Ga$. Also, Tian et al. [28] applied crushed and ball milled arc melted $Ni_{48.8}Mn_{29.7}Ga_{21.5}$ alloy for PECS. Sintering was carried out at 900 °C in a vacuum of 6 Pa under a pressure of 50 MPa for 10 min. According to XRD both the arc melted alloy and the compacted material showed 5M martensitic structure. Martensitic transformation occurred between 7 and 27 °C in the arc melted material and between −15 and 7 °C in the sintered material. The Curie point of both materials was close to 88 °C. Furthermore, the sintered specimen showed magnetic field induced strain of −20 ppm at −10 °C. Similarly to an earlier work by Wang et al. [24], the sintered material had better ductility when compared to the arc-melted material.

The aim of the present work is to explore the possibility of maintaining the properties of the melt-spun ribbons in the bulk by compacting powdered ribbons using pulsed electric current sintering. Two different types of melt-spun powders are used. The bulk samples obtained are then characterized for their structure and properties in the as-sintered state.

2. Materials and methods

Ni–Mn–Ga samples were prepared by arc-melting and melt-spinning at the Magnequench Technology Centre. Two wheel speeds were used to produce: (a) a slowly quenched ribbon (6 m/s) and (b) a rapidly quenched ribbon (23 m/s). These ribbons were lightly crushed to powders with a particle size in the millimeter range. Table 1 details the chemical compositions of the powders determined by ICP spectrometry. According to the Differential Thermal Analysis results, melting of the both powders starts at 1084 °C. DSC measurements revealed the multi-step phase transformation for the 6 m/s sample in temperature range of 70–150 °C, and for the 23 m/s sample at 70–140 °C. According to the XRD measurements, the crystal structure of the 6 m/s powder was non-modulated martensite at room temperature, while the 23 m/s powder exhibited a structure of seven-layered modulated martensite. According to the VSM measurements the saturation magnetization of the powders was reached at about 4 kOe (i.e. 318 kA/m corresponding to about 0.4 T), specifically 3.5 kG for the 23 m/s powder, and 4.0 kG for the 6 m/s powder.

Powders were sintered with the FCT HP D 25-2 pulsed electric current sintering equipment at Aalto University. Processing was carried out in a nitrogen atmosphere at 850 or 875 °C for 8 min with compression of 50 MPa. The dwell time was chosen according to the reduced velocity of the PECS machine piston, which indicated that the sample is close to the full density. Heating rate of 100 °C/min was used up to 100 °C below the processing temperature, and 50 °C/min above this in order to avoid over-shooting of the temperature. The current pulse/pause ratio was 10:5 ms. Disc shaped samples with a diameter of 20 mm and height about 3 mm were made of 8 g of powder. When the samples were extracted from the graphite molds, the surfaces of sintered samples were sand blasted. The surface relief of the finished samples corresponded to the original particle size of the powder (Fig. 1a).

The densities of the sintered and sand blasted compacts were measured by the Archimedes method by weighting the samples to 0.1 mg (Sartorius CPA224S) and assuming theoretical density of 8.1 g/cm^3. The sample surfaces were ground with wet sandpapers to 1200 mesh, polished with the diamond paste (6 μm, 3 μm) and velvet clothes and finally electro-polished in the nitric acid (25%) ethanol bath at −20 °C for 15 s.

The pole figures for the texture analysis were measured at room temperature on the top surface of the samples with the XPert MRD XRD equipment (Co Kα), while the θ–2θ measurements for the crystal structure evaluation were carried out with Phillips PW 3830 apparatus (Cu Kα). The cross section samples for the microstructural, magnetic, and mechanical studies were cut with the diamond saw to the direction determined by the XRD pole figures. The optical study of the samples included the macro evaluation and the metallographic study with the Leica DMRX polarized microscope both at the top surface and the cross section.

The phase and magnetic transitions of the samples were studied by applying the differential scanning calorimeter (Linkam 600; −160 to 300 °C, 5 °C/min) and
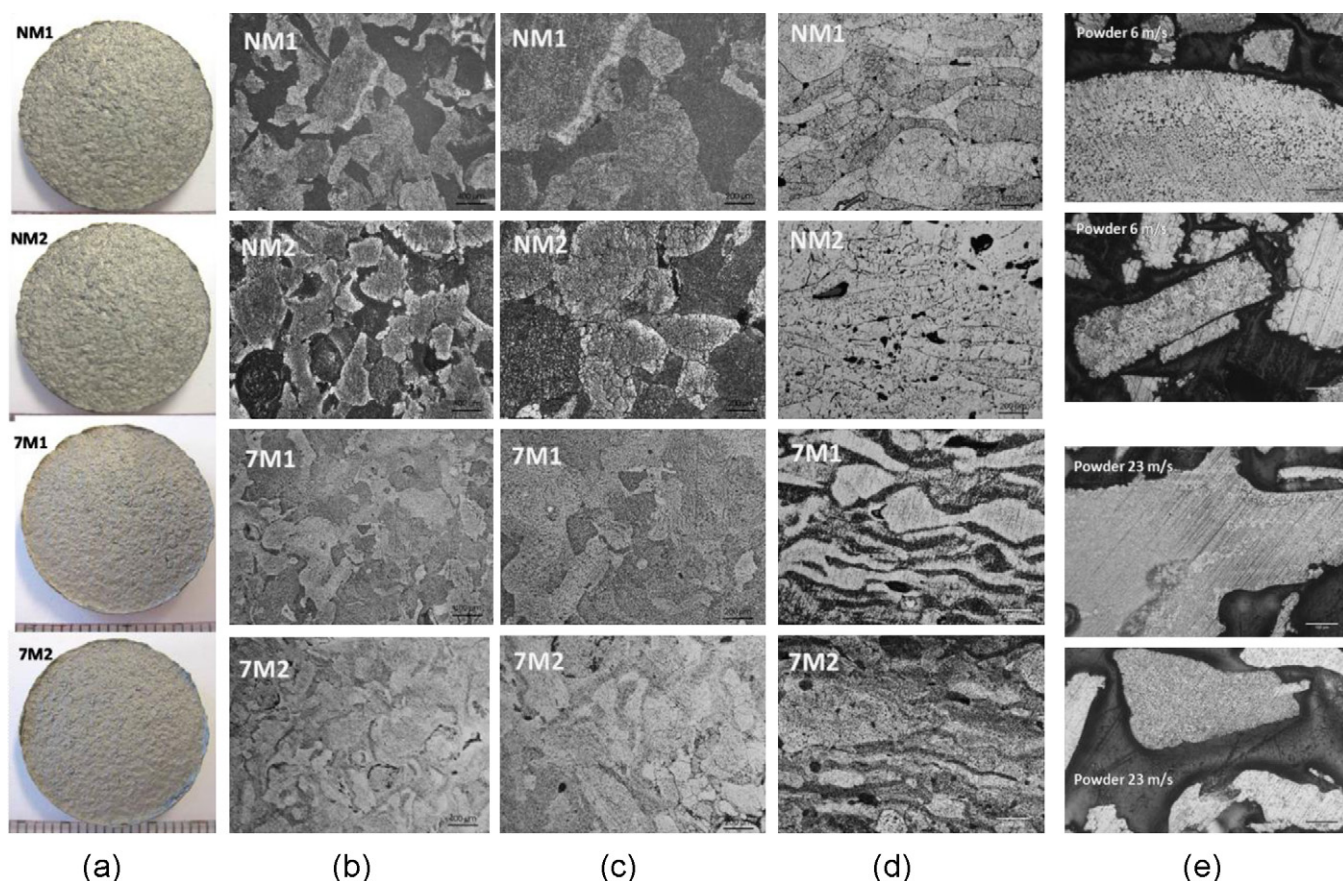
Fig. 1. Structure of the samples *NM*1, *NM*2, 7*M*1, 7*M*2, and powders 6 m/s and 23 m/s. (a) Surface structure of the sand blasted compacts. The top surface microstructure of the compacts in (b) and (c), and (d) the cross section microstructure. (e) Cross section microstructure of the powders.

the magnetic susceptibility measurement (RT 200 °C) with the laboratory made equipment. The magnetization of the samples was evaluated at room temperature with the laboratory-built vibrating sample magnetometer (VSM) with the samples of $3.18 \times 2.67 \times 10.71$ mm^3 and 0.716 g (*NM*1), $2.93 \times 2.65 \times 11.24$ mm^3 and 0.680 g (*NM*2), $1.74 \times 2.55 \times 10.42$ mm^3 and 0.343 g (7*M*1), and $1.85 \times 2.79 \times 14.52$ mm^3 and 0.801 g (7*M*2). The compression behavior was studied with the Lloyd 1000R tensile test machine with samples having dimensions of $2.50 \times 2.80 \times 11.10$ mm^3 (*NM*2) and $5.07 \times 2.80 \times 2.02$ mm^3 (7*M*2).

3. Results

3.1. Density of the compacts

According to the Archimedes measurements the sample with sintering temperature of 850 °C had density of 98.7%, and those compacted at 875 °C showed all above 99% density (Table 1), though some minor porosity can be observed in the optical micrographs of the samples (Fig. 1b–d).

3.2. Structural study of the compacts and the phase transformation temperatures

Though the original powder particle size of millimeter scale was clearly inherited to the sintered compacts as powder particle boundaries (Fig. 1a), the grain size was to some extent influenced by the PECS process. The grain size of the powders (i.e. the original grain size in the ribbons) and the compacts was measured from the optical micrographs (Fig. 1b–e). In powders the grain size depended on the quench wheel speed, being 14 μm on average for ribbons processed at the speed of 6 m/s, and about 5 μm for those processed at 23 m/s. During the PECS average grain size

increased to some extent, being about 21–22 μm for compacts made of powders from the ribbons processed at 6 m/s, and 9 μm for compacts made of the powder from the ribbons processed at 23 m/s.

According to the pole figures the compacted samples showed quite strong texture (Fig. 2). Therefore, it was possible to establish the major [4 0 0] direction of the samples, to which the cutting of the samples for magnetic and mechanical studies was carried out. Samples cut to this direction were tested in VSM. The compressions were made at the [4 0 0] direction.

The crystal structure of the samples at room temperature was a mixture of two martensite types—the non-modulated (NM) and seven-layered modulated (7M) ones (Fig. 3). In samples made of the 6 m/s powder, major fraction of the structure consisted of the non-modulated tetragonal martensite, while samples compacted from 23 m/s powder seven-layered martensite was dominant. The comparison of the peak intensities of the non-modulated and seven-layered martensites at 42° and 44°, yields the phase ratio of the non-modulated/seven-layered structure of the 6 m/s powder, samples *NM*1 and *NM*2, 0.86/0.14, 0.79/0.21, and 0.65/0.35, respectively, and of the 23 m/s powder, and samples 7*M*1, and 7*M*2, 0.11/0.89, 0.21/0.79, and 0.29/0.71 respectively. The phase transformation temperatures and the Curie points were evaluated based on Fig. 4, where several peaks especially for the **NM** samples could be observed. Furthermore, for the NM samples the phase transformations between the cubic phase and the first martensite phase overlaps with the magnetic transition, and the Curie temperatures during heating and cooling are different. The summary of major transition temperatures is given in Table 2.
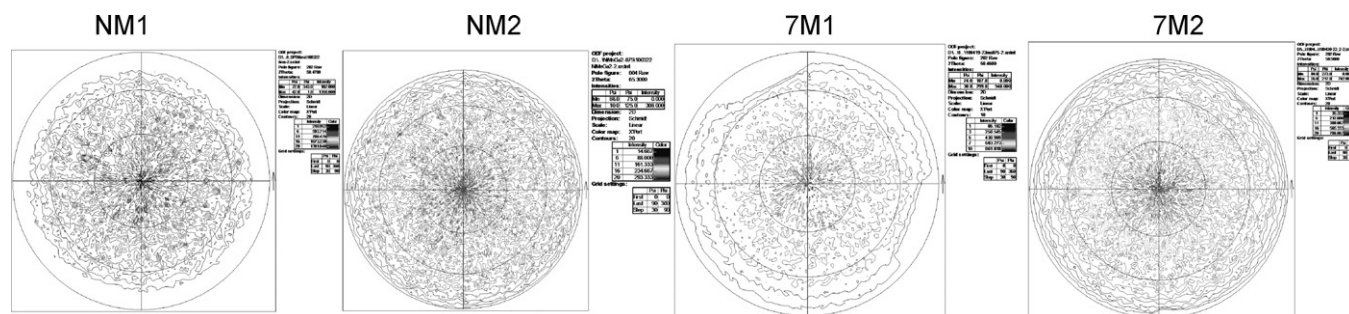
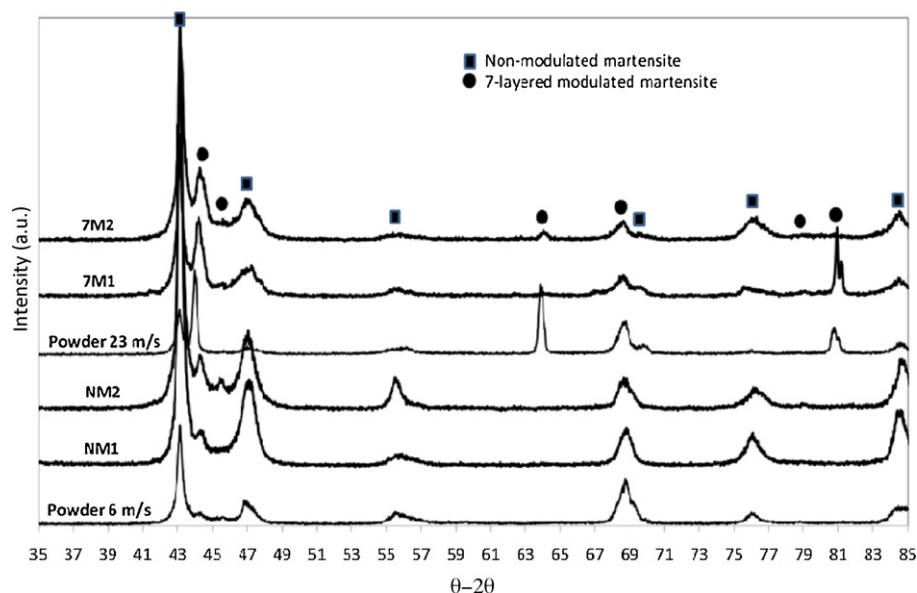**Fig. 2.** Pole figures from the top surface of the samples NM1, NM2, 7M1, and 7M2.

Fig. 3. The θ–2θ diffractograms of the powders, and the compacted samples.

3.3. Magnetic and mechanical behavior of the compacted materials

The VSM results of the compacts are presented in Fig. 5. All the magnetization curves are typical of a soft ferromagnetic material, and no steps that could be associated with the possible martensite twin variant rearrangement were observed. All samples reached the saturation magnetization at about 0.6 T applied field, although minor increase could still be noted until the maximum applied field of 1.2 T. The saturation magnetization (mass) of the NM-samples was nearly the same being 17–19 emu/g. In sample 7M1 there was clearly a higher saturation at about 50 emu/g, although in sample 7M2 it was somewhat lower at around 40 emu/g. In order to compare these values with those given for the respective powders, the magnetization values were converted to A/m using the mass and

volume information of the samples. These were further related to the Gauss values for the top surface and the cross sections as follows: NM1 1.16/1.19 MG, NM2 1.15/1.17 MG, 7M1 2.97/2.89 MG, and 7M2 3.37/3.28 MG, respectively.

The compression test proved that the compacted material was dense and could tolerate quite high stresses in the as-sintered state (Fig. 6). Compression of the sample NM2 showed the ductility of the material as 2% straining was obtained at 289 MPa, and the fracture stress of the material was 326 MPa with the fracture strain of 3.3%. Young's modulus is estimated to be 50 GPa. The results of the compression test with the 7M2 material were not so clear. Because of the sample size the elastic straining region could not be exceeded. The sample showed about 1.5% strain at the 150 MPa stress, and Young's modulus of about 25 GPa.

Table 2
Phase transformation (A_{sx}, A_{fx}, M_{sx}, and M_{fx}) and magnetic transition temperatures (T_C) of the powders and compacts evaluated from the DSC and magnetic susceptibility measurements. Values for the powders are from the provided DSC data.

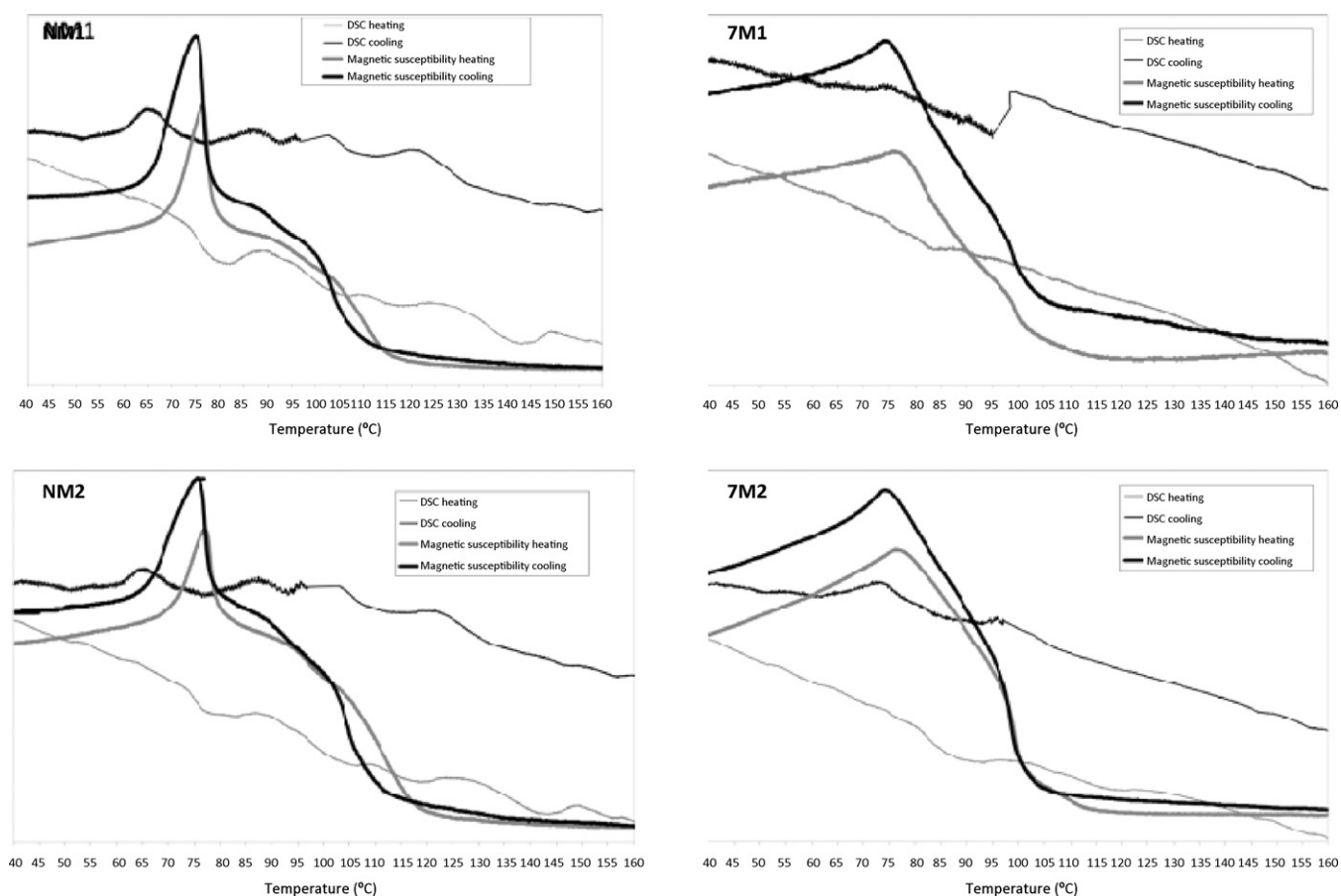|	Heating							Cooling						
	A_{s1} (°C)	A_{f1} (°C)	A_{si} (°C)	A_{fi} (°C)	A_{s2} (°C)	A_{f2} (°C)	T_C (°C)	M_{s1} (°C)	M_{f1} (°C)	M_{si} (°C)	M_{fi} (°C)	M_{s2} (°C)	M_{f2} (°C)	T_C (°C)
Powder 6 m/s	70	90	95	115	135	156		178	155	130	109	105	76	
NM1	73	87	96	122	127	149	107	132	115	112	93	77	60	102
NM2	73	87	96	123	128	149	108	131	117	112	93	77	60	104
Powder 23 m/s	69	104			120	142		116	85			81	68	
7M1	79	96			103	119	102	107	101			80	62	101
7M2	80	98			109	125	100	107	100			84	62	99

Fig. 4. The combined DSC and magnetic susceptibility curves of the compacts.

4. Discussion

The applied PECS processing parameters resulted in dense bulk structures, which exhibited the texture of the melt spun particles, and had microstructural properties similar to the original materials. In general, the crystal structure of the powder was retained in the PECS compacts. Compacts made of the 6 m/s ribbon based material showed mainly the non-modulated martensitic structure, and those made of the 23 m/s ribbon powder showed majority of seven-layered martensitic structure. After compacting at 875 °C, the original grain size had increased from 14 to 22 μm in NM2, and from 5 to 9 μm in 7M1 and 7M2. However, this change was not as large it could have been with the conventional sintering processes with significantly longer processing times [21]. Thus, the structural properties of the powders made from the rapidly quenched ribbons could be preserved in most parts in PECS processing. Choice of the correct processing temperature is of course of major importance. In the present case, compaction temperature of 850–875 °C was selected to ensure that no melting of the material could take place, and the properties of the powders can be preserved. The higher sintering temperature, 875 °C, did provide more dense structure, but resulted in larger grains in the NM samples and it was decided not to increase temperature to 900 °C as in [23]. Future studies can be made for the optimization of the PECS process, investigating the interplay with the dwell time and keeping the pressure and processing temperature at the level applied here.

In [23], a lengthy post-sinter anneal was required to reveal the phase transformation temperatures of the materials. In this study all the transitions could be observed already in as sintered state similarly to [25], although they were spread over a wider temper-

ature region. In the samples having mainly NM structure several peaks were visible in the DSC curves (Fig. 4) pointing to an inhomogeneous structure, where the phase transformations occur at the different temperatures in the different parts of the sample. Therefore, the phase transformation temperatures in Table 2 are regarded as the major transitions of the structure. Some differences between the powders and compacts can be observed—especially at high temperature, while the transition region at lower temperatures seems to be relatively the same. The deviation between the samples is not very large, especially when comparing samples NM1 and NM2. The magnetic transition and phase transformation temperatures overlap in the NM samples resulting in different Curie temperatures during heating and cooling. This phenomenon is known and it has been explained with the different Curie points of the cubic austenite and the non-modulated tetragonal martensite [29,30]. In the magneto-caloric applications, the simultaneous occurrence of the magnetic transition and the phase transformation is needed [16], and thus, the studied materials may have potential in this field, though it is not studied in this work.

The saturation magnetization values given for the powders (3.5–4.0 kG) were to some extent higher than the values of about 2 kG for the $Ni_{52.5}Mn_{24.5}Ga_{23}$ ribbons in [17], but as expected they were clearly lower than the values of the PECS compacts (1.15–3.28 MG). The highest saturation magnetization (mass) of about 50 emu/g, was obtained with the sample 7M1, while the sample 7M2 showed only 40 emu/g. These values are lower than those obtained with a single crystal Ni–Mn–Ga 7M material, for example, with $Ni_{50.5}Mn_{29.4}Ga_{20.1}$ around 60 emu/g ($A m^2 kg^{-1}$) [31], but the difference may be explained with the secondary NM phase in the structure, its fraction being larger in 7M2. The saturation magne-
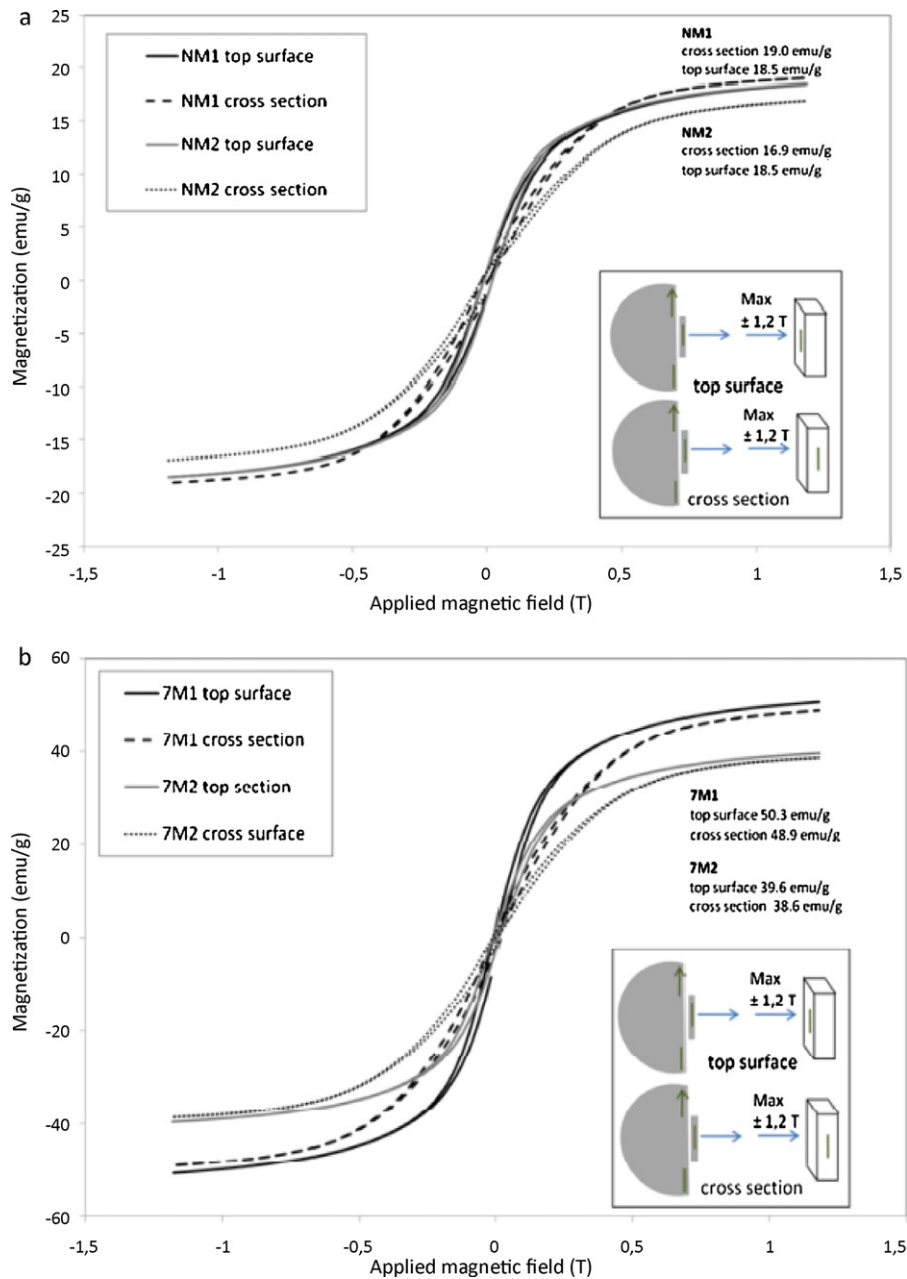
Fig. 5. Magnetization curves for the (a) *NM* samples, and (b) 7*M* samples.

tization (mass) of the non-modulated structure is usually smaller, for example, in [32] it decreases from about 55 to 35 A m^2 kg^{-1} as the *e/a* ratio of the alloy increases from about 7.74 to 7.82. The composition of the powder (appr. Ni$_{56}$Mn$_{24}$Ga$_{20}$) produced from 6 m/s ribbons results in an *e/a* ratio of 7.88, which would explain the observed decrease of the saturation magnetization (mass) of the *NM*-type samples (17–19 A m^2 kg^{-1}) according to [32]. Thus it may be suggested that the major factor in the magnetization of these alloys is actually the Ni content, since the Mn content of the different powders was originally at about the same level.

The compression properties of the studied as-sintered PECS samples are comparable to the results shown for the other kind of martensitic polycrystalline Ni–Mn–Ga materials, although they could not compete with those of sintered and annealed materials as in [24]. The results of the *NM*2 sample fracturing at 326 MPa with the strain of 3.3%, can be compared to the values obtained for the homogenized polycrystalline non-modulated martensitic
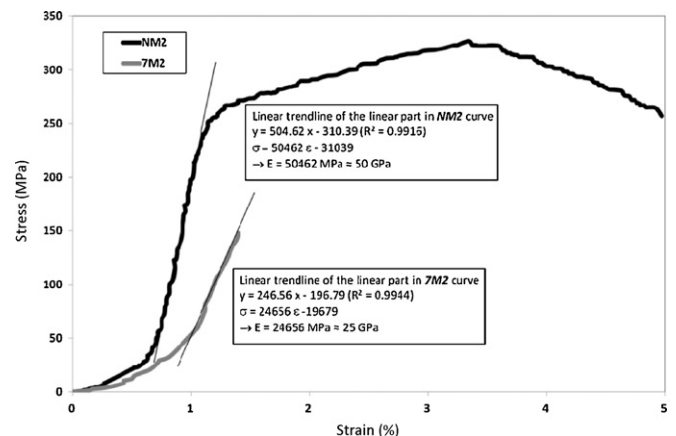

Fig. 6. Compression tests of the *NM*2 and 7*M*2 samples.

Ni$_{54}$Mn$_{25}$Ga$_{21}$ in [33], where the coarse grained (100–200 μm) sample fractured at 440 MPa with 10% elongation, and the fine grained sample (10–50 μm) rod at 970 MPa (16%). These samples obtained the 2% strain at 120 MPa, the stress connected to the twin variant reorientation plateau, while in the present study as-sintered material had clearly higher, 289 MPa, 2% value without any clear stress plateau. In the present work, the 7M2 material was compressed completely elastically. 1.5% strain was obtained at the 150 MPa compression. Its behavior was improved based on the polycrystalline Ni$_{50}$Mn$_{30}$Ga$_{20}$ alloy with the seven-layered modulated martensitic structure [34], as the [1 0 0] sample fractured already at about 140 MPa with only 1% strain. This behavior was significantly improved by applying training of material [33]. When comparing the slopes of the stress–strain curves in Fig. 6, the estimations for the Young's modulus from the Hooke's law gives 50 GPa for the NM2 and 25 GPa for the 7M2 sample. These values are comparable with those of the sintered sample presented in [25].

Based on the obtained results with the as-sintered PECS samples it is clear that the powder grain size could be preserved in the compacts. For the future work, it would be beneficial if their properties to carry out certain post-treatment of the materials could be evaluated. The long-duration annealing enhances the functional properties and defines the phase transformation temperatures [1]. Also, some kind of mechanical training procedure could improve the functional properties [33]. However, as the original ribbon material shows already very promising structure, the post-treatments should be carried out with care. If successful, the 7M structure may offer useful magnetic shape memory performance.

5. Conclusions

Pulsed electric current sintering was used to compact two Ni–Mn–Ga powders made of ribbons fabricated at different quench speeds. The grain size of the powders increased somewhat during the sintering at 875 °C with 50 MPa for 8 min. The as spun powders contained both the non-modulated and seven-layered modulated martensite structures, and these were inherent in the compacts. Sintering seemed to increase the amount of the phase that originally was in minority. The non-homogenized sintered materials showed relatively similar transformation behavior to the raw material powders. The textured compacts showed good mechanical properties in compression testing. Despite the compacts being heavily textured, their polycrystalline structure showed ferromagnetic behavior with the best saturation magnetization being ∼50 emu/g for the seven-layered dominant structure. The results of the present work suggest that with the correct type of melt-spun powder composition and quench rate, it is possible to obtain compacts with desirable properties.

Acknowledgements

References

[1] O. Söderberg, Y. Ge, I. Aaltio, O. Heczko, S.-P. Hannula, Mater. Sci. Eng. A 481–482 (2008) 80–85.
[2] I. Aaltio, Y. Ge, X. Liu, O. Söderberg, J. Tellinen, A. Sozinov, S.-P. Hannula, in: G.B. Olson, D.S. Lieberman, A. Saxena (Eds.), Proceedings of ICOMAT '08TMS, 2009, pp. 627–631.
[3] I. Aaltio, A. Soroka, Y. Ge, O. Söderberg, S.-P. Hannula, Smart Mater. Struct. 19 (2010) 075014.
[4] P. Müllner, V.A. Chernenko, G. Kostorz, J. Appl. Phys. 95 (2004) 1531–1536.
[5] H.B. Xu, Y. Li, C.B. Jiang, Mater. Sci. Eng. A 438–440 (2006) 1065–1070.
[6] L. Pareti, M. Solzi, F. Albertini, A. Paoluzi, Eur. Phys. J. B 32 (2003) 303–307.
[7] D.L. Schlagel, Y.L. Wu, W. Zhang, T.A. Lograsso, J. Alloys Compd. 312 (2000) 77–85.
[8] G. Erdelyi, H. Mehrer, A.W. Imre, T.A. Lograsso, D.L. Schlagel, Intermetallics 15 (2007) 1078–1083.
[9] R.W. Overholser, M. Wuttig, D.A. Neuman, Scripta Mater. 40 (1999) 1095–1102.
[10] I. Aaltio, O. Söderberg, M. Friman, I. Glavatskyy, Y. Ge, N. Glavatska, S.-P. Hannula, in: P. Šittner, L. Heller, V. Paidar (Eds.), Proceedings of ESOMAT EDP Sciences (www.esomat.org), 2009, doi:10.1051/esomat/200904001.
[11] J.J Croat, J. Appl. Phys. 81 (1997) 4804–4809.
[12] D.N. Brown, Z. Chen, P. Guschl, P. Campbell, J. Magn. Magn. Mater. 303 (2006) e371–e374.
[13] N. Dearing, A.G. Jenner, IEEE Trans. Magn. 42 (2006) 78–80.
[14] S.-H. Guo, Y.-H. Zhang, J.-L. Li, Y. Qi, B.-Y. Quan, X.-L. Wang, Chin. Phys. Lett. 23 (2006) 227–230.
[15] J. Gutiérrez, P. Lázpita, J.M. Barandiarán, M.L. Fdez-Gubieda, J. Chaboy, N. Kawamura, J. Magn. Magn. Mater. 316 (2007) e610–e613.
[16] N.V. Rama Rao, R. Gopalan, M. Manivel Raja, J. Arout Chelvane, B. Majumdar, V. Chandrasekaran, Scripta Mater. 56 (2007) 405–408.
[17] N.V. Rama Rao, R. Gopalan, V. Chandrasekaran, K.G. Suresh, J. Alloys Compd. 478 (2009) 59–62.
[18] V.A. Chernenko, G.N. Kakazei, A.O. Perekos, E. Cesari, S. Besseghini, J. Magn. Magn. Mater. 320 (2008) 1063–1067.
[19] A.K. Panda, A. Kumar, M. Ghosh, A. Mitra, J. Magn. Magn. Mater. 320 (2008) e730–e733.
[20] M. Lahelin, I. Aaltio, O. Heczko, O. Söderberg, Y. Ge, B. Löfgren, S.-P. Hannula, J. Seppälä, Composites: Part A 40 (2009) 125–129.
[21] R. Orrù, R. Licheri, A.M. Locci, A. Cincotti, G. Cao, Mater. Sci. Eng. R 63 (2009) 127–287.
[22] M.E. Cura, R. Ritasalo, U. Kanerva, J. Syrén, J. Oksanen, J. Lotta, T. Suhonen, J. Lagerbom, O. Söderberg, E. Turunen, S.-P. Hannula, Sintering of TiC-Ultimet powders by pulsed electric current sintering and effect of the Ultimet content on the microstructure and mechanical properties, in: Proceedings of PM2010, European Powder Metallurgy Association, 2010, Art. 367.
[23] Z. Wang, M. Matsumoto, T. Abe, K. Oikawa, J. Qiu, T. Takagi, J. Tani, Mater. Trans. JIM 40 (1999) 389–391.
[24] Z. Wang, M. Matsumoto, T. Abe, K. Oikawa, T. Takagi, J. Qiu, J. Tani, Mater. Trans. JIM 40 (1999) 863–866.
[25] M. Matsumoto, M. Ohtsuka, H. Miki, V.V. Khovailo, T. Takagi, Mater. Sci. Forum 394–395 (2002) 545–548.
[26] M. Matsumoto, T. Takagi, J. Tani, T. Kanomata, N. Muramatsu, A.N. Vasil'ev, Mater. Sci. Eng. A 273–275 (1999) 326–328.
[27] Z. Wang, M. Matsumoto, T. Abe, K. Oikawa, J. Qiu, T. Takagi, J. Tani, Mater. Sci. Forum 327–328 (2000) 489–492.
[28] X.H. Tian, J.H. Sui, X. Zhang, X. Feng, W. Cai, Martensitic transformation, mechanical property and magnetic-field-induced strain of Ni–Mn–Ga alloy fabricated by spark plasma sintering, J. Alloys Compd. 509 (2011) 4081–4083.
[29] V.V. Khovailo, T. Takagi, J. Tani, R.Z. Levitin, A.A. Cherechukin, M. Matsumoto, R. Note, Phys. Rev. B: Condens. Matter Mater. Phys. 65 (2002) 092410.
[30] V.A. Chernenko, V.A. L'vov, S.P. Zagorodnyuk, T. Takagi, Phys. Rev. B: Condens. Matter Mater. Phys. 67 (2003) 064407.
[31] L. Straka, O. Heczko, K. Ullakko, J. Magn. Magn. Mater. 272–276 (2004) 2049–2050.
[32] O. Heczko, L. Straka, J. Magn. Magn. Mater. 272–276 (2004) 2045–2046.
[33] U. Gaitzsch, M. Pötschke, S. Roth, B. Rellinghaus, L. Schultz, Scripta Mater. 57 (2007) 493–495.
[34] S. Roth, U. Gaitzsch, M. Pötschke, L. Schultz, Adv. Mater. Res. 52 (2008) 29–34.